Fizika Nizkikh Temperatur, 2010, v. 36, No. 7, p. 790–796

Effect of Ca(Ce) doping on thermopower of $LaMnO_3$ manganites

Dinesh Varshney[1,2], Irfan Mansuri[1], and A. Yogi[1]

[1] *School of Physics, Vigyan Bhawan, Devi Ahilya University, Khandwa Road Campus, Indore 452001, India*
E-mail: vdinesh33@rediffmail.com; vdinesh33@gmail.com

[2] *School of Instrumentation, USIC Bhawan, Devi Ahilya University, Khandwa Road Campus, Indore 452001, India*

Received November 5, 2009, revised December 24, 2009

With a view to explain the thermoelectric effects of $La_{0.8}Ca_{0.2}MnO_3$ and $La_{0.8}Ce_{0.2}MnO_3$ polycrystalline samples and to seek the role of scattering mechanism, a systematic investigation of thermopower $S(T)$ in the metallic phase have been undertaken. Within the relaxation time approximation, it is noticed that, the phonon drag $S(T)$ with scattering of phonons from defects, grain boundaries, phonons and charge carriers in these samples are effective in the metallic regime. Later on, Mott expression is employed to incorporate the carrier diffusive thermopower. The temperature dependence of the $S(T)$ is determined by competition among the several operating scattering mechanisms for the heat carriers and a balance between carrier diffusion and phonon drag contributions in the polycrystalline samples of $La_{0.8}Ca_{0.2}MnO_3$ and $La_{0.8}Ce_{0.2}MnO_3$.

PACS: 73.50.Lw Thermoelectric effects;
74.25.Kc Phonons;
75.47.Gk Colossal magnetoresistance;
75.47.Lx Magnetic oxides.

Keywords: thermoelectric effects, phonons, colossal magnetoresistance, manganites.

1. Introduction

The perovskite material $R_{1-x}A_xMnO_3$ (R being trivalent rare earth ions) can be either hole doped or electron doped depending on whether A is a divalent alkaline earth ion such as Ca, Ba, Sr, Pb etc or tetravalent such as Ce, Sn etc. Both classes of this material exhibit a rich phase diagram as a function of temperature, magnetic field and doping, and show interesting phenomenon like colossal magnetoresistance (CMR) and metal–insulator transition [1,2]. Double-exchange interaction via spin polarized conduction electrons is appreciated as the main cause of CMR.

The existence of metallic conduction and ferromagnetism in manganites below the metal–insulator transition temperature has been explained by invoking the double exchange (DE) mechanism between Mn^{3+} and Mn^{4+} states [3]. On the other hand, the DE mechanism is inappropriate in explaining the spin-lattice or charge-lattice interactions, i.e., Jahn–Teller (JT) interaction and polarons, which is effective in addressing the electrical transport in the high temperature-semiconducting phase [4]. We thus aimed in measuring and understanding the transport of underdoped $La_{0.8}Ca_{0.2}MnO_3$ and $La_{0.8}Ce_{0.2}MnO_3$ manganites in the low temperature, i.e., in the metallic phase.

The thermopower is one of the powerful and sensitive transport probes in analyzing the charge carrier dynamics as it manifests the local moments of charge carriers [5]. Infact, one can predict the nature of charge carriers based on the degree of JT interaction [6], studies on CMR phenomenon of manganites have been focussed [6–8]. The thermopower measurements and its sign yield vital information about the type of charge carriers responsible for the conduction mechanism of CMR materials. In view of this, thermopower studies of CMR materials are very important and also interesting.

A direct microscopic evaluation of the phonon drag thermopower is an open issue yet. It has been shown [9] that phonon drag thermopower is substantial in manganites further provides the motivation of the present investigation. The thermopower depends on the way the heat carriers interact with one another and with the environment namely the possible interaction of phonons with defects, grain boundaries and by themselves. It is worth to stress that in the above-mentioned studies [8,9], the importance of the competition among the several operating scattering mechanisms and a balance between the phonon drag and carrier diffusive contributions have not been stressed,

however these are expected to be substantial to clarify the heat transfer. Apart from phonon drag effects another possible explanation for thermoelectric power in manganites is due to scattering of electrons by spin waves. In ferromagnets and antiferromagnets, the electron-magnon interaction produces magnon drag [8].

Relatively less studied in this respect are the electron-doped manganites of the form $La_{1-x}Ce_xMnO_3$. If Ce ions exist in a mixed-valent state with a valence between 3 and 4 as in the electron-doped superconductors, then Mn ions are expected to be Mn^{3+}/Mn^{4+} instead of Mn^{3+}/Mn^{2+}, and the excess electrons provided by Ce doping are responsible for the metallic conduction and ferromagnetism. This raises the possibility of CMR occurring in system with a mixed-valent state of Mn^{2+} and Mn^{3+} and therefore one expects these to have certain unique properties. Thus, a detailed understanding of the transport properties is essential for electron and hole doped manganites.

We have chosen polycrystalline divalent Ca-doped $La_{0.8}Ca_{0.2}MnO_3$ and tetravalent Ce-doped $La_{0.8}Ce_{0.2}MnO_3$ manganites as to have the comparison of $S(T)$ and to improve our understanding of the interplay of scattering processes between the heat carriers themselves and between the carriers and the impurities in the liquid He_2 to N_2 temperature region. We admit that no systematic efforts have been made in the past. Further it is relevant to study the relative magnitudes of these scattering processes, which lead to the anomalous behaviour. The results we report here do indeed shed some very important light on the nature of phonon and carrier channel of thermopower in manganites.

2. Sample preparation and experimental details

The polycrystalline divalent Ca-doped $La_{1-x}Ca_xMnO_3$ and tetravalent Ce-doped $La_{1-x}Ce_xMnO_3$ ($x = 0.2$) samples were prepared by solid-state synthesis. Stoichiometric amounts for La_2O_3, $CaCO_3$, CeO_2, and MnO_2 were mixed and heated at different temperatures (950, 1050, 1250 and 1350 °C) in air for 24 hours with intermediate grindings. The pellets were finally annealed at 1000 °C in oxygen atmosphere.

The thermopower measurement of the doped manganites compounds has been done liquid He_2 to liquid N_2 temperature range using two-stage close cycle refrigerator. The thermopower sample holder consists of two copper blocks electrically insulated from rest of the system but thermally connected to the cold head of close cycle refrigerator. The radiation shield and the vacuum of 10^{-5} mbar ensure the minimal heat leak. The temperature of the one block is measured using silicon diode sensor with Lakeshore temperature controller. The sample is kept in between the copper blocks. A finite temperature difference of 1–2 K is maintained between the two copper blocks by manganin wire heater wounded on the copper blocks and controlled using Au–Fe (7%) — Chromel thermocouple and Lakeshore temperature controller. The thermo-emf thus developed across the sample is measured against copper. The thermopower is computed as the ratio of thermo-emf to the temperature difference. The absolute thermopower is then calculated by subtracting the measured thermopower from the copper thermopower which has the value of few μV/K in the whole temperature range [10].

3. Results and discussion

The variation of thermopower with temperature is illustrated in Fig. 1 for both polycrystalline samples from liquid He_2 to liquid N_2 temperature range. It is inferred that the thermopower shows a metallic phase, for both $La_{0.8}Ca_{0.2}MnO_3$ and $La_{0.8}Ce_{0.2}MnO_3$. The thermopower measurements at low temperatures for underdoped $La_{0.8}Ca_{0.2}MnO_3$ and $La_{0.8}Ce_{0.2}MnO_3$ yield positive sign and thus holes are the type of charge carriers responsible for the conduction mechanism consistent with the earlier measurements for $La_{1-x}Ce_xMnO_3$ ($x \le 0.6$) [11]. Furthermore, in low temperature domain, S shows upturn in the ferromagnetic phase and might be due to the weak localization. A linear term and a phonon-drag-type anomaly are clearly visible at low temperatures, further evidence of well-established metallic phases.

We have attempted to interpret the observed behaviour in this temperature region following a model where the phonons are described in the Debye model and the hopping of charge carriers are treated in an isotropic double exchange model. The use of the Debye model is reasonable since the temperature region of interest lies well below the Debye temperature. As the simplest approximation to the problem at hand, the isotropic Debye model approach is used to derive qualitative results, as we will demonstrate later. We start with a model Hamiltonian that follows [12,13]

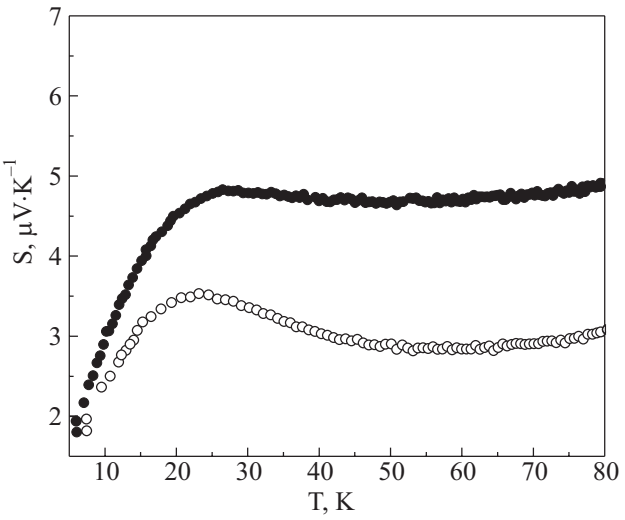

Fig. 1. Thermopower as a function of temperature for the $La_{0.8}Ca_{0.2}MnO_3$ (○) and $La_{0.8}Ce_{0.2}MnO_3$ (●).

$$H = \sum_k \varepsilon_k a_k^+ a_k + \sum_q \omega_q b_q^+ b_q + \sum_{k_1,k_2} \phi(k_1,k_2) a_{k_1}^+ a_{k_2} + D_p \sum_{k,q} q \left[\frac{\hbar}{2\rho\omega_q}\right]^{1/2} a_{k+q}^+ a_k (b_k + b_{-k}^+) +$$

$$+ \frac{R}{2N} \sum_{q_1,q_2} e^{i(q_1+q_2)r_i} \left[\frac{\hbar\omega_{q_1}\hbar\omega_{q_2}}{4}\right]^{1/2} (b_{q_1} - b_{-q_1}^+)(b_{q_2} - b_{-q_2}^+) + H_{\text{ph-ph}}, \quad (1)$$

here, initial two terms is carriers and phonon excitations. The third and fourth terms represent the carrier–impurity interactions and carrier–phonon interactions, respectively. The fifth and sixth terms denote the phonon–impurity and the phonon–phonon interaction, respectively.

The notations a (a^+) and b (b^+) are the creation (annihilation) operators for phonons and carriers. D_p is the deformation-potential constant and R is the relative ionic-mass difference [$(M''–M)/M''$], respectively. The phonon frequency of a wave vector q is ω_q. N is the number of cells. ρ is being the mass density of ions and R_i stands for the position of defects. ε_k is the hole free energy.

The thermopower following model Hamiltonian [Eq. (1)] can be calculated from the Kubo formula [14]. It has contributions from both the phonons and the carriers. We first explore the lattice part; in the continuum approximation [15]

$$S_{\text{ph}}^{\text{drag}}(T) = -\frac{k_B}{|e|}\left[\frac{T}{\theta_D}\right]^3 \int_0^{\omega_D} d\omega(\beta\omega)^4 A(\omega)(\beta\omega)^4 \frac{e^{\beta\omega}}{(e^{\beta\omega}-1)^2}, \quad (2)$$

with k_B is the Boltzmann constant, e is the charge of carriers, ω_D is the Debye frequency and $\beta = \hbar/k_BT$. The relaxation time is inhibited in $A(\omega)$ and is proportional to the imaginary part of the phonon self-energy. The phonon drag thermopower relaxation time $A(\omega)$ is written as

$$A(\omega) = \left[1/\tau_{\text{ph}-d} + 1/\tau_{\text{ph}-gb} + 1/\tau_{\text{ph}-\text{ph}}\right]^{-1} \times$$

$$\times \left[1/\tau_{\text{ph}-d} + 1/\tau_{\text{ph}-gb} + 1/\tau_{\text{ph}-\text{ph}} + 1/\tau_{\text{ph}-c}\right]. \quad (3)$$

In the weak interaction case, it has been calculated to the lowest order of the various interactions. The relaxation times are expressed as

$$1/\tau(\omega) = 2\left|\text{Im}\, P(\omega/v_s, \omega)\right|. \quad (4)$$

The various relaxation times are defined in terms of transport coefficients as [12,13]

$$\tau_{\text{ph}-d}^{-1}(\omega) = D_{\text{ph}d}(\hbar/k_B)^3\omega^4, \quad (5)$$

$$\tau_{\text{ph}-gb}^{-1}(\omega) = D_{\text{phg}b} v_s / L, \quad (6)$$

$$\tau_{\text{ph}-\text{ph}}^{-1}(\omega) = D_{\text{phph}}\left(T\omega\hbar/k_B\right)^3, \quad (7)$$

and

$$\tau_{\text{ph}-c}^{-1}(\omega) = D_{\text{ph}c}\omega n_F, \quad (8)$$

where L is the crystal dimension, n_F is the Fermi–Dirac distribution function. The notation $\tau_{\text{ph}-d}$, $\tau_{\text{ph}-gb}$, $\tau_{\text{ph}-\text{ph}}$ and τ_{ph-c} are the phonon scattering relaxation time due to defects, grain boundaries, phonon and phonon–carrier interactions, respectively. It is worth to mention that to this order Mathiessen's rule holds namely, that the inverse of the total relaxation time is the sum of the various contributions for the different scattering channels. The transport coefficients appearing in Eqs. (5)–(8) are defined as

$$D_{\text{ph}d} = \left[\frac{3n_iR^2}{4\theta_D^3}\right] \quad (9)$$

and

$$D_{\text{ph}c} = \frac{9\pi}{4}\left[\frac{m}{3M}\right]^{1/2} \frac{{D_p}^2}{\varepsilon_F^2} \quad (10)$$

characterize the strengths of the phonon–defects and phonon–electron scattering process. Here, n_i is the density of impurities or defects, ε_F is the Fermi energy of holes as carriers and m is its mass.

Let us now proceed to include the effect of free carrier diffusion contribution towards thermopower contribution employing the well-known Mott formula. The low temperature carrier diffusion thermopower [15] is

$$S_c^{\text{diff}}(T) = -\frac{\pi^2 k_B^2 T}{3|e|}\left[\frac{\partial \ln\sigma(\varepsilon)}{\partial\varepsilon}\right]_{\varepsilon=\varepsilon_F} \quad (11)$$

with $\sigma(\omega)$ (= $Ne^2\tau(\varepsilon_F)/m$) is the energy dependence of conductivity in the relaxation time approximation. In what follows, the mean free path of the carriers (ℓ) is assumed to be independent of temperature, the Eq. (11) becomes

$$S_c^{\text{diff}}(T) = -\frac{\pi^2 k_B^2 T}{3|e|\varepsilon_F} \quad (12)$$

with constant mean free path, the method point to the scattering of carriers by impurities is dominant. In the temperature range where diffusive S dominates, the S of metals, even disordered ones, is of the order of a few $\mu V \cdot K^{-1}$ and is linear in temperature. The thermopower of semiconductors, in contrast, is typically several tens to hundreds of $\mu V \cdot K^{-1}$, and is governed by thermal activation of carriers

thus increasing with decreasing temperature. Henceforth, the S of metals and nonmetals differ not only in their magnitude but also in their temperature dependence. It is further noticed that both these samples shows positive thermopower range up to liquid N_2 and is an indicative of holes as charge carriers for thermal conduction.

For the actual calculation of the transport properties, it is essential to know realistic values of some physical parameters governing the thermopower behavior. To gain additional insight into the mechanism responsible for the transport we have carried out thermopower studies with particular emphasis on carriers and phonon drag contribution for $S(T)$ in manganites. The acoustic mode frequencies are estimated using a inverse-power overlap repulsive potential whose details are reported elsewhere [16].

While calculating the Debye temperature θ_D the index number of the repulsive potential is used as s = 10 and the in plane Mn–O distance r_0 = 1.94 [1.96] Å, yielding $\kappa = 15.4[15.2]\cdot10^4$ g·m·s^{-2} for $La_{0.80}Ca_{0.20}MnO_3$ [$La_{0.80}Ce_{0.20}MnO_3$], respectively. Details of the method of calculation of characteristic frequencies and their relevant expressions are reported elsewhere [16]. It is useful to point out that for manganites the index number of the repulsive potential has been reported [17] to be s = 10. With these parameters, the Debye temperature (θ_D) is estimated as 410 (412) K for $La_{0.80}Ca_{0.20}MnO_3$ ($La_{0.80}Ce_{0.20}MnO_3$), respectively, which is consistent as those revealed from specific heat measurements [18]. It is worth to mention that θ_D is a function of temperature and varies from technique to technique and its value also vary from sample to sample with an average value and standard deviation of $\theta_D = \theta_D \pm 15$ K. For $La_{0.80}Ca_{0.20}MnO_3$ ($La_{0.80}Ce_{0.20}MnO_3$), we use the transport coefficients that characterize the strengths of the phonon–defects D_{phd} (10^{-8} K^{-3}) is 6.12 (5.4), phonon–grain boundary D_{phgb} (10^{-3}) 3.3 (3.4), phonon–phonon D_{phph} (10^{-4} K^{-6}·s^{-1}) 0.5 (0.7) and phonon–carrier D_{phe} (10^{-3}) 3.1 (8.5) scattering process, respectively. These are indeed material dependent parameters for phonon drag thermopower in the present model. In these calculations we have used the length of the sample is about 3 mm and $v_s = 3\cdot10^5$ cm·s^{-1}.

Let us first discuss the relative magnitudes of the various scattering mechanisms. A plot of various scattering phonon relaxation time as a function of $x = \hbar\omega/k_BT$ in terms of frequency at T = 10 and 50 K are shown in Figs. 2 and 3 for $La_{0.80}Ca_{0.20}MnO_3$ and $La_{0.80}Ce_{0.20}MnO_3$, respectively. It can be seen that for low value of x, the phonon–electron scattering is higher while for high value of x, it is the phonon–defect scattering that grows faster. On the other hand, at both small and large value of x, phonon–phonon scattering process is weaker at low temperatures (T = 10 K) for both the samples. As we go with increase in temperature (T = 50 K) phonon–phonon scattering improves and phonon–electron scattering becomes weaker. In particular, phonon–phonon umklapp scattering grows faster than phonon–electron scattering due to large mobility of carriers in the high temperature region.

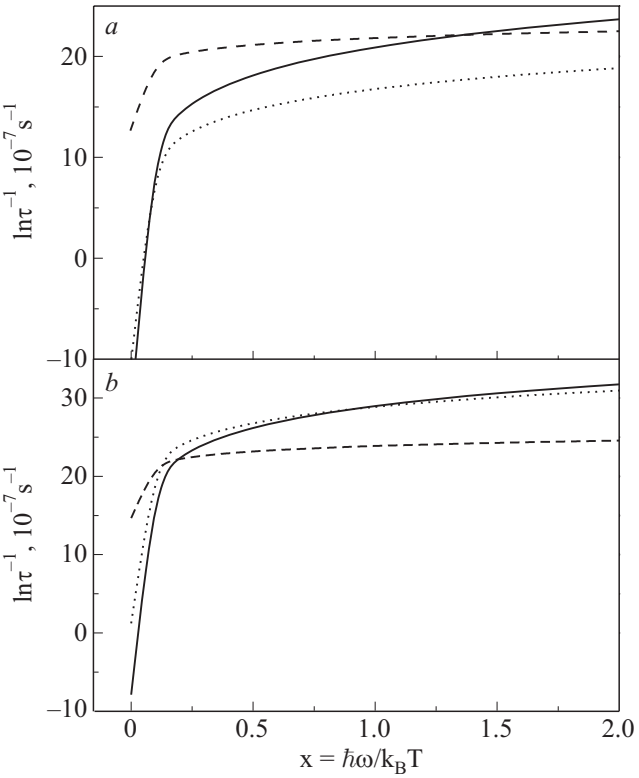

Fig. 2. Various phonon relaxation times at different temperatures: 10 K (*a*) and 50 K (*b*) as a function of $x = \hbar\omega/k_BT$ for the $La_{0.8}Ca_{0.2}MnO_3$: ph–*d* (—), ph–*c* (---), ph–ph (⋯).

The main finding of phonon drag thermopower (S_{ph}^{drag}) in Fig. 4 is that at low temperatures and they cannot scatter phonons. S_{ph}^{drag}, thus, increases exponentially with temperature in the absence of the other scattering mechanism. Although the phonon drag thermopower experiences an exponential increase at low temperature, the presence of the defect, grain boundaries and the carriers set a limit on its growth, as a consequence the phonon drag thermopower diminishes as the temperature increases further.

It is evident from Fig. 5 that at low temperatures, $S_{ph}^{drag}(T)$ is linear in temperature, which is common for most metals and change in a slope around 10 K. The departure from linearity at about 10 K depends on the relative magnitudes of the phonon defect and phonon–phonon interactions. Below 10 K, the grain boundary and defects become the effective phonon scatterers and the thermopower exhibits a typical T^2 behavior at even lower temperatures, grain-boundary scattering dominates and the usual Debye T^3 behavior is revealed. $S_{ph}^{drag}(T)$ shows a saturating behaviour and shows slow negative $dS(T)/dT$ at higher temperatures. This kind of nature is attributed to the fact that the phonons mean free path decreases with the increase in temperature, as more and more carriers are available for scattering. Possible reason for the departure from linearity

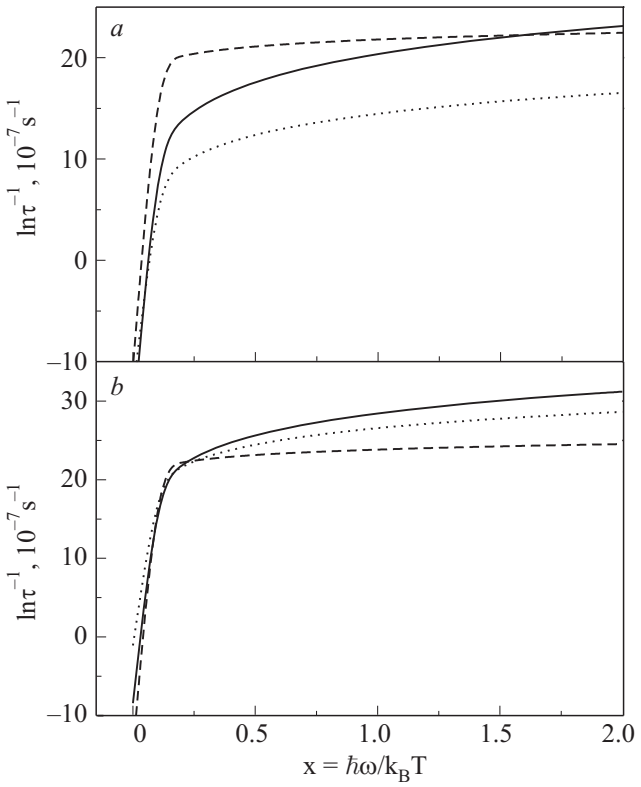

Fig. 3. Various phonon relaxation times at different temperatures 10 K (*a*) and 50 K (*b*) as a function of $x = \hbar\omega/k_BT$ for the $La_{0.8}Ce_{0.2}MnO_3$: ph–*d* (—), ph–*c* (---), ph–ph (⋯).

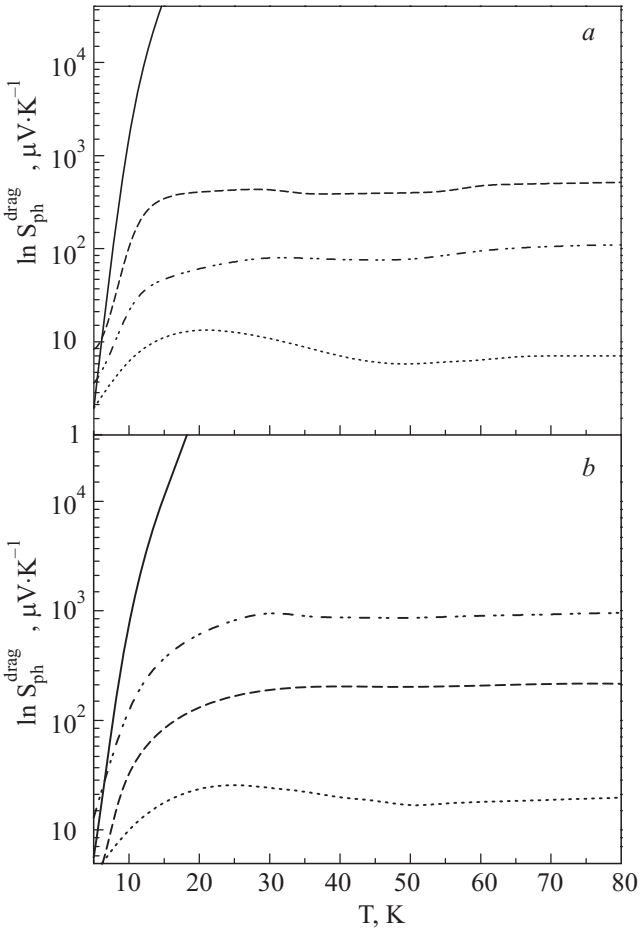

Fig. 4. Variation of phonon thermopower as function of temperature in presence of various phonon scattering mechanism for the $La_{0.8}Ca_{0.2}MnO_3$ (*a*) and $La_{0.8}Ce_{0.2}MnO_3$ (*b*): *d* (—), *d* + *gb* (---), *d* + *gb* + *c* (–⋯–), *d* + *gb* + *c*+ph (⋯).

at about 10 K is mainly due to the competition between the increase in the phonon population and decrease in phonon mean free path due to phonon-phonon scattering as evident from Eqs. (2) and (3).

To ascertain the physical significance of the density of impurities, we evaluate the transport coefficients D_{phd} appeared in Eqs. (8) and (9). We estimate the product of density of impurities and square of relative ionic mass difference, n_iR^2 = 5.0 (1.3) for $La_{0.8}Ca_{0.2}MnO_3$ ($La_{0.8}Ce_{0.2}MnO_3$), respectively, from the value of coefficient D_{phd}. Due to the fact that the transport parameter D_{phd} is determined by the magnitude of the phonon–impurity interaction, we are able to roughly estimate the density of impurity scatterers which may point to the fact that the quasi particles in the metallic state are essentially localized. By this way, one can set a limit to the concentration of impurities if the impurities as scatterers are of isotope in origin.

We turn now to the calculation of the carrier diffusion thermopower (S_c^{diff}) which is given by the Eqs. (11) and (12). The effective mass of the carriers along the Mn–O plane is obtained from the electronic specific heat coefficient, γ, using the relation, $m^* = 3\hbar\gamma d / \pi k_B^2$. Considering γ = = 4.7 mJ/mol/K^2 from the heat capacity measurement for $La_{0.80}Ca_{0.20}MnO_3$ [18], $m^* \cong 2.4\ m_e$ is obtained. For a stack of 2D conducting planes well separated by an average spacing, *d*, the condition for optimised transfer of electrons infers the 2D electronic charge carrier density and follows $n_cd^2 = 1$ to obtain $n_c \cong 2.2\cdot10^{14}$ cm^{-2}. Analogously, we express 3D electronic charge carrier density following $n_vd^3 = 1$ to obtain $n_v \cong 5.65\cdot10^{21}$ cm^{-3}. Within the Fermi liquid picture the calculated electron parameter as the Fermi energy $\varepsilon_F \cong 0.6$ eV for $La_{0.80}Ca_{0.20}MnO_3$ system. To gain an additional insight in to the observed metallic, it is worth to address the possible role of mass renormalization of carriers due to differed values of γ obtained from specific heat measurements [18] and electron energy band structure calculations [19]. In this situation it is worth to address the role of Coulomb correlations in revealing the transport properties in manganites. The effective charge carrier mass is sensitive to the nature of interaction in Fermi liquid description.

In the present analysis of elastic carrier-impurity contribution to the thermopower at low temperatures is documented in Fig. 5 for $La_{0.80}Ca_{0.20}MnO_3$ and $La_{0.80}Ce_{0.20}MnO_3$ along with the measured data. The thermopower behavior depends on the competition among the various scattering mechanisms for the heat carriers and balance between the

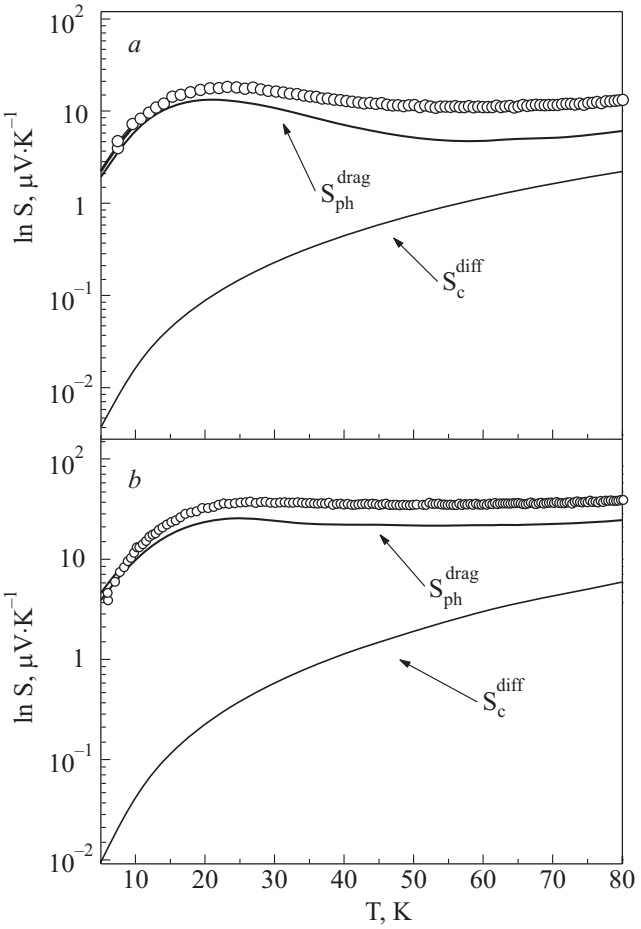

Fig. 5. Thermopower versus temperature along with experimental data for $La_{0.8}Ca_{0.2}MnO_3$ (*a*) and $La_{0.8}Ce_{0.2}MnO_3$ (*b*). S_{total} (—), S_{exp} (○).

electron and phonon competition. Finally, it is worth stressing that the $S(T)$ decrease slowly above 25 K and is well reproduced from the present theoretical model (see Fig. 5), this phenomenon is attributed to shortened phonon mean free path as compared to that at low temperatures. It may be seen that the slope change in S_{ph}^{drag} is much more pronounced than that in S_c^{diff} below 15 K for both samples. The reason for being this change is due to the fact that the phonon–impurity scattering dominates and electron–impurity scattering is weaker.

4. Conclusions

The low-temperature heat transfer, i.e., thermopower behavior is an instructive probe to reveal the lattice effects and carrier diffusion as well the interaction of these excitations with one another with impurities, grain boundaries and defects. We have measured thermopower of Ca and Ce doped $LaMnO_3$ manganites and analysed the metallic behavior within the framework of relaxation time approximation. The thermopower measurements for underdoped $La_{0.8}Ca_{0.2}MnO_3$ and $La_{0.8}Ce_{0.2}MnO_3$ reveals a positive sign and thus holes are the type of charge carriers responsible for the conduction mechanism.

In order to simulate the actual situation occurring in the temperature dependent behavior of $S(T)$ in manganites, we considered two channels to $S(T)$: carrier diffusion (S_c^{diff}) and phonon drag (S_{ph}^{drag}) is discussed within the Debye-type relaxation rate approximation in terms of the acoustic phonon frequency, a relaxation time τ and the sound velocity. The rapid increase in $S(T)$ is attributed to increase in phonon mean free path due to carrier condensation in the low temperature domain limited by various impurity scattering mechanism. The physical entities in the present scheme that characterize the strengths of the phonon–defect, phonon–electron, and phonon–phonon scattering leads to a result that successfully retrace the experimental curve. The behavior of the $S(T)$ is determined by competition among the several operating scattering mechanisms for the heat carriers and a balance between carrier diffusion and phonon drag contributions in the polycrystalline samples of hole-doped $La_{0.8}Ca_{0.2}MnO_3$ and electron doped $La_{0.8}Ce_{0.2}MnO_3$ manganites.

Acknowledgements

Authors are thankful to UGC– DAE CSR, Indore and to Dr. V. Ganesan for their support in carrying out thermopower measurements. Financial assistance from MPCST, Bhopal, India is also gratefully acknowledged. One of us IM acknowledges CSIR, New Delhi for the award of senior research fellowship.

1. A.P. Ramirez, *J. Phys.: Condens. Matter* **9**, 8171 (1997).
2. P. Raychaudhuri, S. Mukherjee, A.K. Nigam, J. John, U. Vaisnav, and R. Pinto, *J. Appl. Phys*. **86**, 5718 (1999); C. Mitra, P. Raychaudhuri, J. John, S.K. Dhar, A.K. Nigam, and R. Pinto, *J. Appl. Phys*. **89**, 524 (2001).
3. C. Zener, *Phys. Rev*. **82**, 403 (1951).
4. A.J. Millis, *Phys. Rev*. **B53**, 8434 (1996).
5. F.J. Blatt, P.A. Schroeder, C.L. Foiles, and D. Greig, *Thermo Power of Metals*, New York, Plenum (1976).
6. B. Chen, C. Uher, D.T. Morelli, J.V. Mantese, A.M. Mance, and A.L. Micheli, *Phys. Rev*. **B53**, 5094 (1996).
7. S. Yamada, T. Amira, H. Ikeda, and K. Takita, *J. Phys. Soc. Jpn.* **69**, 1278 (2000).
8. P. Mandal, *Phys. Rev*. **B61**, 14675 (2000).
9. M. Jaime, M.B. Salamon, K. Pettit, M. Rubinstein, R.E. Treece, J.S. Horwitz, and D.B. Chrisey, *J. Appl. Phys. Lett*. **68**, 1576 (1996); M. Jaime, P. Lin, M.B. Salamon, and P.D. Han, *Phys. Rev*. **B58**, R5901 (1998).
10. L.S. Sharath Chandra, A. Lakhani, D. Jain, S. Pandya, P.N. Vishwakarma, M. Gangrade, and V. Ganesan, *Rev. Scientific Instrum*. **79**, 103907 (2008).
11. S. Das, A. Poddar, B. Roy, and S. Giri, J. *Alloys and Compounds* **365**, 94 (2004).
12. Dinesh Varshney, K.K. Choudhary, and R.K. Singh, *New J. Phys*. **5**, 72 (2003).

13. Dinesh Varshney and N. Kaurav, *J. Low Temp. Phys*. **147**, 7 (2007).
14. J. Callaway, *Quantum Theory of the Solid State*, Academic Press, London (1991).
15. N.F. Mott and E.A. Davis, *Electronic Processes in Non-Crystalline Materials*, Clarendon, Oxford (1979).
16. Dinesh Varshney and N. Kaurav, *Eur. Phys. J.* **B37**, 301 (2004).
17. Dinesh Varshney and N. Kaurav, *Eur. Phys. J.* **B40**, 129 (2004).
18. L. Ghivelder, I.A. Castillo, N.M. Alford, G.J. Tomka, P.C. Riedi, J. MacManus-Driscoll, A.K.M. Akther Hossain, and L.F. Cohen, *J. Magn. Magn. Mater*. **189**, 274 (1998).
19. W.E. Pickett and D.J. Singh, *Phys. Rev*. **B53**, 1146 (1996).